journal of the mechanical behavior of biomedical materials 116 (2021) 104363

Contents lists available at ScienceDirect

Journal of the Mechanical Behavior of Biomedical Materials

journal homepage: http://www.elsevier.com/locate/jmbbm

Compositional, microstructural and mechanical effects of NaCl porogens in brushite cement scaffolds

Erdem Şahin [a,*], Muhsin Çiftçioğlu [b]

[a] Department of Metallurgical and Materials Engineering, Muğla Sıtkı Koçman University, Muğla, Turkey
[b] Department of Chemical Engineering, İzmir Institute of Technology, İzmir, Turkey

A B S T R A C T

Modification of the setting process of brushite cements by varying the concentration of ions that alter calcium phosphate crystallization kinetics, is known to enable control on the monetite conversion extent and the accompanying microporosity. This is useful because monetite serves as a suitable matrix in macroporous scaffolds due to its higher phase stability and finer crystal morphology compared to its hydrous counterpart brushite. In this study the synergistic effect of NaCl and citric acid on the microstructural evolution of brushite cement was demonstrated and microporosity of macroporous monetite-rich cement blocks was minimized by a variable NaCl porogen size distribution approach. Initially, maximum packing ratio of various combinations of NaCl size groups in PEG were determined by their rheological analysis in a range between 57% and 69%. Statistical analysis revealed a positive correlation between the amounts of NaCl particles under 38μm and 212μm and the maximum packing ratio. Further broadening the size distributions of NaCl porogens with fine cement precursors was effective in increasing the solids packing ratio of cement blocks more than the maximum packing ratio for the porogens. This improvement in packing was accompanied by a reduction in microporosity despite the increase in micropore volume with ion induced monetite formation. The detrimental effect of the microporosity introduced to the structure during monetite formation was balanced for some size distributions and not so much for others, thereby resulting in a wide range of porosities and mechanical properties. Thus, the exponential dependence of mechanical properties on porosity and the mechanical properties of monetite-rich macroporous blocks at the theoretical zero-porosity were determined according to Rice's model. Zero-porosity extrapolations were much higher than those predicted for brushite cement, contrary to the common assumption that brushite is mechanically stronger than monetite.

1. Introduction

Calcium phosphate cements (CPCs) are versatile bioactive ceramics that form workable pastes through dissolution of one or more calcium phosphates in aqueous setting solution and the subsequent precipitation of stable calcium phosphates (Şahin, 2018). The development of monetite forming cements has attained considerable traction in CPC literature as alternatives to brushite forming cements which have drawbacks in bioresorbablity (Gbureck et al., 2007; Klammert et al., 2009) and the associated osteoinductivity (Geffers et al., 2015; Tamimi et al., 2012a) Monetite, dicalcium phosphate anhydrous - the dehydrated form of brushite, dicalcium phosphate dihydrate, has a finer crystal structure (Sivakumar et al., 1998), higher specific surface area (Tamimi et al., 2012b), and a more constant, controllable resorption rate *in vivo* (Gbureck et al., 2007; Tamimi et al., 2012a) compared to brushite which is known to transform to an insoluble hydroxyapatite layer. Its osteoinductivity is closely related to these beneficial surface features (Tamimi et al., 2008, 2010). Formation of metastable monetite is facilitated by kinetic parameters that influence the order of precipitation of CPCs: temperature (Galea et al., 2008), pH (Bohner et al., 2000), ionic strength (Sahin and Ciftcioglu, 2013) and water content (Gbureck et al., 2005). The only drawback of monetite cement that results in its mechanical weakness (Ajaxon et al., 2017; Desai et al., 2007) is the extra 19% microporosity forming as a result of the shrinkage ($\rho_{monetite} = 2.9 > \rho_{brushite} = 2.34$ g/cm^3) during setting reaction (Öhman et al., 2015). The intrinsic strength of monetite crystals free of voids has not been documented yet. The relatively higher hardness (3.5 vs 2.5 on Mohs scale (www.mindat.org/min-2755; www.mindat.org/min-793)) of the mineral forms is an indication that the denser monetite structure is indeed stronger than bursite. This hypothesis is validated in this study by estimation of the zero-pore strength according to Rice's theory on the exponential dependence of the mechanical properties of ceramics on macroporosity (Rice, 1998) and by minimizing the intrinsic micropororsity of monetite blocks.

Calcium phosphate cements are highly loaded ceramic suspensions until complete dissolution and crystallization of the precursors in water when they transform to elastic bodies with packing defects containing water reserviors (Liu et al., 2006). These reservoirs act as stress intensifiers depending on their geometry and size, and should be filled by various means of compaction. Microporosity is defined in this context as

* Corresponding author.
E-mail addresses: erdemsahin@mu.edu.tr (E. Şahin), muhsinciftcioglu@iyte.edu.tr (M. Çiftçioğlu).

https://doi.org/10.1016/j.jmbbm.2021.104363
Received 31 October 2020; Received in revised form 19 January 2021; Accepted 21 January 2021
Available online 1 February 2021

the intrinsic porosity that forms during the cement setting process through these processes. Pores that are produced by the addition of large porogens with the intention of creating biologically relevant interconnected conduits ranging in diameter from 10 to a few hundred micrometers are considered as macropores. Micropores in CPCs typically accounting for as much as 45% of the volume (Dorozhkin, 2008) are not as useful as coarse conduits which provide more efficient biological transport and cellular interaction (von Doernberg et al., 2006; Jones et al., 2009). Micropores are mainly useful in controlled drug delivery systems where macromolecules or microspheres are adsorbed on cement voids during the setting process (Espanol et al., 2009).

Size distribution of cement precursors has been shown to effectively improve packing of brushite cement blocks and reduce microporosity to a quarter of the expected value when unisized precursors are used (Bentz et al., 1999; Hofmann et al., 2009). While wider particle size distribution improves the compaction of cements (Espanol et al., 2009), narrow particle size distribution is known to increase cement setting rate (Aiqin et al., 1997). Packing of cement precursor particles is more efficient in the presence of the aqueous setting medium (Frigione and Marra, 1976) which lubricates solid particles, dissolve and suspend them, decreasing the formation of solid agglomerates and mats that result in low packing densities. Another effect of the setting liquid that infiltrates the nano to micrometer sized packing defects is continuous precipitation of nano-sized cement end product and the resulting reconfiguration of the micropore size distribution to submicron range (Kwan and Fung, 2009) and an overall improvement in packing.

It is virtually impossible to completely eliminate all packing defects that form during CPC setting due to the limited lubricating effect of water. Therefore physical approach of compaction does not suffice to maximize the strength of CPC scaffolds while forming macropores in the matrix for higher cement resorption and bioactivity and complimentary techniques are necessary. The common approach in the scaffold design has been improving the strength of the cement matrix, chemically by modifying the composition (Takagi and Chow, 2001; Xu and Quinn, 2002) or by incorporation of reinforcements (Xu et al., 2001; Canal and Ginebra, 2011). The present work aims to both physically and chemically modify the CPC microstructure through utilization of NaCl, both as an effective controller of the phase stability in acidic cements with citric acid, and as porogens of variable size distribution that may form interconnected conduits at optimum size distributions. The distinct and synergistic compositional, morphological and mechanical effects of various NaCl size groups were monitored to effectively tailor the microstructure, composition and strength of monetite-rich CPC blocks that could support a large volume of macropores.

2. Materials and methods

2.1. Preparation of microporous monetite-rich CPC blocks

Brushite forming cement of the following stoichiometry was set in cylindrical PTFE molds to produce blocks containing intrinsic microporosity:

$$\beta\text{-}Ca_3(PO_4)_2 + Ca(HPO_4)2.H_2O + 7H_2O \rightarrow 4CaHPO_4.2H_2O \quad (1)$$

or

$$\beta\text{-}Ca_3(PO_4)_2 + Ca(HPO_4)2.H_2O \rightarrow 4CaHPO_4 + H_2O \quad (2)$$

Stoichiometric amount of precursors (β-TCP, Sigma 21,218, d_{50} = 7.7 μm, monocalcium phosphate monohydrate, Sigma C8017, d_{50} = 30 μm as measured in reagent grade ethanol by laser granulometry (Malvern Mastersizer 3000), with Ca/P ratio of 1 were set in the presence of 3 wt% monetite seeds (Sigma, d_{50} = 24 μm), 0.3M aqueous citric acid (Sigma 77-92-9) solution and various NaCl (Merck 106,404) concentrations at a powder/liquid ratio of 2.5. The ionic strength of deionized water with 0.3M citric acid was varied by addition of various concentrations of NaCl between 0 and 6M. A total of 5 samples were produced for each run by mixing the precursors on a vortex shaker oscillating at a frequency of 40 Hz for 1 min and casting in homemade PTFE molds of dimensions of 20 mm height and 10 mm diameter. Samples were further compacted during setting by the weight of 1 kg steel block resting on the plunger of the cylindrical molds for 1 h. Set samples were aged in humidifying oven at 30 °C and 85% relative humidity for 72 h and later characterized for mechanical, microstructural and compositional features.

2.2. Determination of the maximum packing ratio of size distributed NaCl mixtures

Theoretical maximum packing ratio of porogen particles with different size distributions were obtained by rheological analysis in the presence of a liquid polymer binder. Thirty eight sets of size distributed NaCl mixtures were carefully selected to represent all possible size distribution combinations by a 6-factor fractional factorial experimental design. NaCl particles were distributed to six size groups by size reduction using mortar and pestle for 5 min and the successive sieving in stainless steel meshes with 38, 53, 75, 106, 150, 212 μm sized openings. Generally interaction between different particle size groups are known to be significant at size ratios less than 7 (Kalyon and Aktaş, 2014) and their potential negative effects on packing was aimed to be investigated in this study by employing the six size groups spanning the ratio range 1–7. Coarse powder on the sieve with 212 μm openings was discarded and the rest were used as 6 distinct size groups, the size distribution of which was measured in ethanol by Mastersizer 3000. Statistically significant size distributions for effective packing were aimed to be determined in the rheometry analysis by variation of the amounts of NaCl size groups. Size distributed NaCl mixtures were dispersed in 5 ml of Polyethylene glycol 200 (Merck 817,001), a low viscosity liquid polymer, at solid loadings of 10%, 20%, 30%, 40% and 50% by volume in triplicate runs.

After manual mixing of the suspensions for 10 min, well-dispersed suspensions were analyzed in a rotational rheometer (Haake Mars III) for shear stress and viscosity as functions of shear rate. Rheological analysis of PEG200-NaCl suspensions was done at the shear rate range 0.1–500 1/s. Viscosity readings were done for all samples at a rate of 200 1/s. This rate was sufficiently high to obey model assumptions and sufficiently low to prevent phase separation and slip at high rates. Viscosity values obtained at each solid loading were used to determine the maximum packing density as a function of solid loading according to the empirical model equation developed by Liu et al. (Liu, 2000):

$$\eta_r = [a(\varphi_{max} - \varphi)]^{-2} \quad (3)$$

where η_r is the relative viscosity calculated by the ratio of the suspension viscosity to binder viscosity, φ_{max} is the maximum packing ratio, φ is the solid loading and a is a constant obtained by graphically plotting the following relation:

$$1 - \eta_r^{-1/2} = a\varphi + b \quad (4)$$

where a is the slope and b is the intercept of the curve. At the boundary condition of $\varphi = \varphi_{max}$, relative viscosity reaches infinity, $1 - \eta_r^{-1/2}$ equals 1 so that one can determine the maximum packing ratio at that point graphically as shown in Fig. 1.

Initially, variations of viscosity of pure PEG200 and its NaCl suspensions with shear rate were obtained in order to calculate the relative viscosity values. As seen in Fig. 1a, increasing the solid content had the effect of increasing the shear-thinning character of the suspension as expected due to particle interations. For high solid loadings the liquid polymer had the tendency to separate from NaCl at high shear rates greater than 300 1/s. The viscosity curve was seen to reach a plateau region at high shear rates for samples without phase separation.

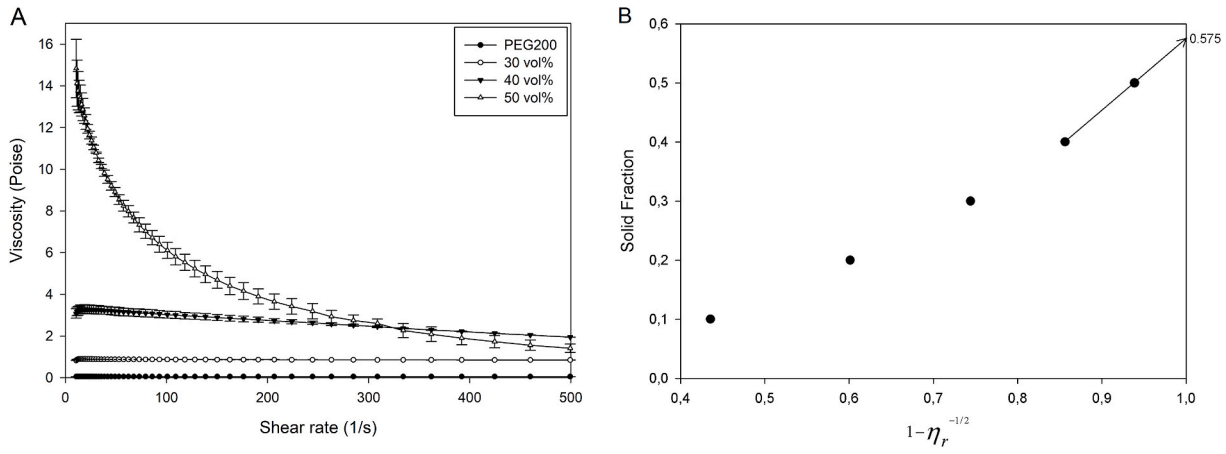

Fig. 1. a) Variation of viscosity of PEG200 and NaCl suspensions of various volume ratio with shear rate, (b) and the variation of relative viscosity of sample 16 with solid fraction, the arrow pointing to the maximum packing fraction.

Viscosity values taken at 200 1/s shear rates were both sufficiently low to simulate the shear rate conditions of cement mixing and sufficiently close to the constant viscosity value reached at the plateau region. Fig. 1b shows that the linear trendline intersecting the 40% and 50% solid loading was used for the calculation of maximum packing ratio since Liu's model is only applicable to suspensions with high solid loading.

2.3. Preparation of macroporous monetite-rich CPC blocks

Macroporous cement block samples produced in this study were designed to fit the maximum packing data obtained from the rheometric analysis of the porogen particles. Maximum packing ratio values obtained for different NaCl size distributions were used to adjust the NaCl porogen volume for cement block samples with constant cement precursor amount to obtain constant sample volume. As given in the supplementary data, unit volumes of the cement blocks have to vary if constant porogen amount is used in preparation, as the packing densities of each porogen group differ. Conversely, to obtain dimensionally similar samples with comparable mechanical properties, i.e., to compensate for the change in micropore volume due to anticipated efficient packing, porogen amount was adjusted according to the maximum packing ratio.

In order to observe the effect of the variation in solid particle size distribution on sample physical properties, equal amounts of cement precursors were added to each porogen group studied rheometrically. Cement blocks were prepared by mixing 1.13 g β-Tricalcium phosphate (β-TCP, Sigma 21,218, d_{50} = 7.7 μm), 0.86 g Monocalcium phosphate monohydrate (MCPM, Sigma C8017, Sigma, d_{50} = 30 μm), 0.07 g monetite seed (DCPA, Sigma, d_{50} = 24 μm) and various amounts of size distributed porogens in polyethylene syringes with a diameter of 12 mm on a vortex shaker oscillationg at a frequency of 40 Hz for 1 min in order to improve packing. Subsequent addition of 0.51 ml of 0.2 M aqueous citric acid solution at a cement powder/liquid ratio of 4 was again done in the presence of vibration for 1 min. Samples were further compacted during setting by a weight of 1 kg resting on the plunger of the cylinders for 1 h. Final setting times were reached typically 20 min after mixing as reported elsewhere (Şahin and Kalyon, 2017), so that the cement samples were viscous enough during the initial minutes of compaction for reconfiguration of the solid particles under applied compaction pressure.

Set cement blocks were aged in PP syringe molds for 72 h at room temperature. Cylindrical samples were carefully removed from the molds and each one was leached by keeping in an aluminum basket in 1 L of agitated ultrapure water by for 24 h for complete removal of porogens. Wet, macroporous cement blocks were subjected to Archimedean water intrusion test. These samples were later dried in vacuum oven at a pressure of 10^{-2} mbar and 30 °C for 72 h. Dry cement blocks were subsequently tested in the extensometer for compressive strength. Fractured samples were further characterized by semi-quantitative XRD and SEM as explained in the following sections.

2.4. Porosity evaluation

Samples were subjected to porosity evaluation subsequent to leaching in deionized water for 72 h. Sample volume, density, and porosity were determined by Archimedes' water intrusion method at room temperature using the standard density kit by Mettler Toledo. Volume measurements by Archimedean method is prone to errors especially due to mass losses during sample molding, demolding and handling. To minimize the errors, a reproducible sample preparation process by which equal molding periods, and compaction forces were applied to all 228 samples was used. Six samples for each of 38 sets were leached in deonized water for equal durations prior to Archemedian analysis and the arithmetic means of their porosities were taken as the representative values.

2.5. Compositional analysis

After destructive mechanical tests, fractured cements were subjected to phase analysis by XRD. Compositional analysis of set and dried cement samples by powder XRD was conducted using Philips X'Pert Pro powder diffractometer with Cu K_α radiation at a generator voltage of 45 kV, and a tube current of 40 mA. All XRD patterns were obtained at a scan range of 5–60°, scan step size of 0.05 and 5 s per step. Semi-quantitative analysis was performed according to the external standard method utilizing corundum as explained in detail in the supplementary data.

2.6. Mechanical analysis

Upon leaching of the salt, wet samples were dried in vacuum oven at 30 °C and 10^{-2} mbar for 120 h prior to mechanical testing. Low temperature drying was applied to prevent conversion of brushite to monetite and generation of microporosity after compaction. Although dry storage at ambient conditions has been reported to induce monetite conversion (Ajaxon et al., 2017), relatively short duration of drying in the present study is assumed to not contribute significantly to phase evolution. Compressive strength of dry samples were determined in an Shimadzu AG-I 250 kN universal testing extensometer at a crosshead speed of 1 mm/min. The resolution of stroke was 0.001 mm and the resolution of force was 1 N. Ultimate compressive strength, yield

strength and elastic moduli of cylindrical cement blocks were measured according to the ASTM C 773 standard. The sensitivity of mechanical properties to the total porosity of cement blocks necessitates small tolerance to variations in sample porosity in order to compare their mechanical properties. Sample dimensions showed slight variations up to 10% from the 2:1 height/diameter ratio suggested by the standard for compressive testing of porous ceramics and the resultant standard deviations are accounted for in the analysis of mechanical properties. The macroporous samples generally exhibited quasi-ductile behavior and strained up to 0.3. It should furthermore be noted that dry strength of samples will not represent the exact performance of the materials *in vivo* due to the absence of water that generally negatively affects the structural integrity of cements.

2.7. Morphological analysis

Microstructural analysis of selected samples were done by using Philips XL-30S FEG scanning electron microscope. Their fracture surfaces were sputter coated with gold prior to examination with secondary electron detector at an accelerating voltage of 5.00 kV and wedge distance of 10 mm.

2.8. Statistical analysis

Experimental design of the rheological analysis was done using the statistical analysis software Design Expert by Statease. A six factor fractional factorial response surface design was employed and the significant parameters were determined using one-way analysis of variance. Also the results obtained from the Archimedean, microstructural and mechanical analysis of cement samples were analyzed by using one-way analysis of variance. A p value less than 0.05 was considered as statistically significant. Post-hoc tests were not applied due to the low number of statistically significant model terms.

3. Results & discussions

3.1. Correlation between the microstructure and mechanical properties of microporous monetite-rich blocks

Setting products of the cement blocks prepared by utilizing citric acid and various NaCl concentrations were determined by XRD analysis, and the compositional data was correlated with the data from Archimedean and compressive testing. Monetite (DCPA) formation in preferrence to brushite (DCPD) was observed for samples set with liquid containing 0.3M citric acid and NaCl above a critical concentration of 3M (see supplementary information for detailed data). Monetite formation extent improved above a NaCl concentration of 3M and maximised at a NaCl concentration of 6M. Similarly high monetite contents have been reported by Cama et al. and Şahin et al. by saturating the setting liquid of brushite cement with respect to NaCl (Cama et al., 2013; Sahin and Ciftcioglu, 2013). It is evident from the XRD results that monetite and brushite exist in intimate contact in the set cement blocks at all NaCl concentrations studied. The simultaneous presence of brushite at the highest NaCl concentration may be attributed to fluctuations in saturation due to dilution of the setting liquid with water excluded from MCPM and monetite during dissolution and crystallization. The lower ionic strength of the diluted liquid in the vicinity of monetite crystals is also expected to increase supersaturation of brushite and facilitate its nucleation.

The micrographs of brushite-rich and monetite-rich samples are given in Fig. 2. Brushite crystals are characteristically smooth and prismatic while monetite crystals form in a stacked-sheets morphology in the presence of excess NaCl. Although not visible in the micrographs, the main calcium source in the cement microstructure, β-TCP residue was also seen to increase with NaCl concentration. In the absence of any ionic modifier β-TCP is seen to dissolve completely in aqueous cement setting liquid with time (Bohner and Gbureck, 2008). As reported previously, the ionic modifiers reduce the solubility of β-TCP and brushite while kinetically enabling monetite precipitation in place of brushite (Şahin and Çiftçioğlu, 2014). In addition, water excluded from monetite has a dilution effect on the pH of the setting liquid, further increasing the pH and lowering β-TCP dissolution. Higher residual β- TCP amount is thus attributed to its lower solubility at high ionic strength in the presence of citric acid. Conversely, high solubility of MCPM is seen not to be affected by high ionic strength as it was not detected through compositional and morphological analyses. Its crystals are unstable in contact with water and is assumed to completely dissolve within the first few minutes of setting.

Stability of brushite at low NaCl concentrations and stability of monetite at high NaCl concentrations makes the phase evolution a sigmoidal function of ionic strength (which is a linear function of NaCl concentration) with a sudden variation at the intermediate NaCl concentration around 3M as seen in Fig. 3. Apparently NaCl concentration is an effective phase control parameter in brushite cements. As NaCl has a solubility of 6.143M in water at room temperature, brushite cement scaffolds containing NaCl porogen for the purpose of inducing macroporosity will undergo phase transition, the extent of which may depend on the ionic strength of local water reserviors in the microstructure. If NaCl particles are well dispersed so that the ionic strength is high uniformly throughout the structure, a significant portion of the cement matrix will transform to monetite upon employing NaCl porogen and the accompanying exclusion of water from the crystals will increase the

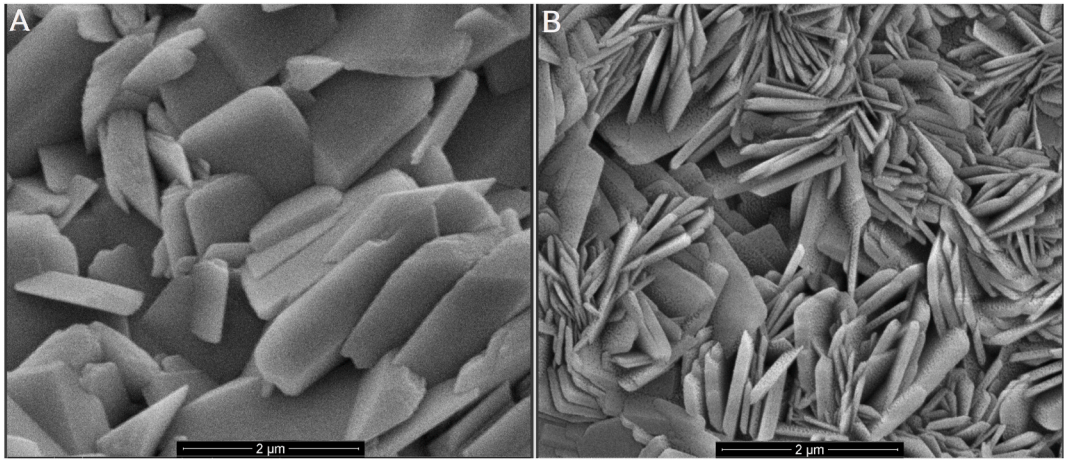

Fig. 2. Micrographs of a) brushite and b) monetite phases formed from the β-TCP-MCPM prescursors

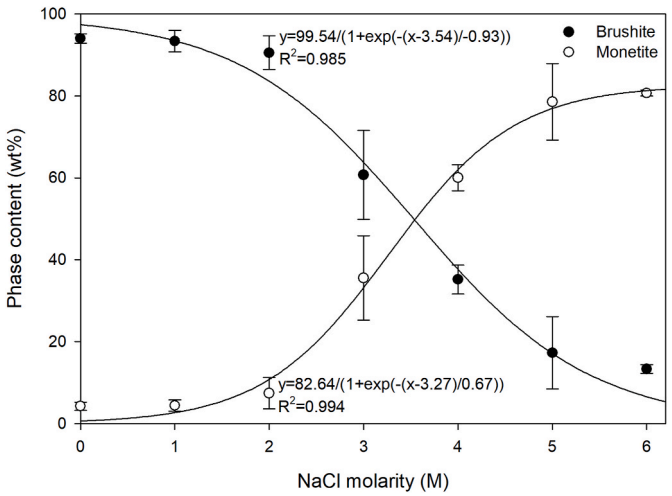

Fig. 3. Variation of brushite and monetite contents with increasing NaCl concentration of the setting liquid.

microporosity considerably.

The typical inorganic cement microstructure seldomly include large spherical or ellipsoidal pores and interparticle microporosity in the nanoscale is present. These so called colloidal pores have been found to account for about 90% of total porosity volume (Kendall et al., 1983; Alshaaer et al., 2011). Mechanical properties of inorganic cements are dependent on the length of the crack-like macropores and the volume fraction of the colloidal pores. In brushite crystal structure, lattice water molecules are interlayered between the calcium phosphate chains and monetite crystal structure is denser than brushite due to the exclusion of water molecules (Wang and Nancollas, 2008). Thus, formation of monetite is accompanied by a gradual increase in colloidal porosity such that it is linearly dependent on monetite amount. For this study the dependence of porosity on monetite content is expressed in Fig. 4a as:

$$P\% = 0.194[M\%] + 36.5 \quad (5)$$

where P% is the volume percent porosity and M% is the weight percent monetite content. Here 36.5% is the intrinsic microporosity of brushite cement without monetite, which corresponds to a solid packing density of 63.5% that is within the range obtained from the random packing of monosized spheres.

The correlation between porosity and the compressive strength of the samples follows an exponential curve in accord with the theory of Rice on the fracture mechanics of ceramics:

$$\sigma = \sigma_0 e^{-bP} \quad (6)$$

where σ_o is zero-porosity strength, σ is the strength at porosity ratio P, and the constant b is the stress concentration factor that is mainly dependent on pore morphology (Rossi, 1968). Constant b depends on the geometry of the pores and is typically between 0.04 and 0.07 for most ceramics with regular ellipsoidal pore morphology (Liu, 1998). Larger macropores are also known to intensify the stress more than smaller macropores (Liu et al., 2006). Studies on mechanical properties of calcium phosphates reported a range of b values between 0.035 and 0.108

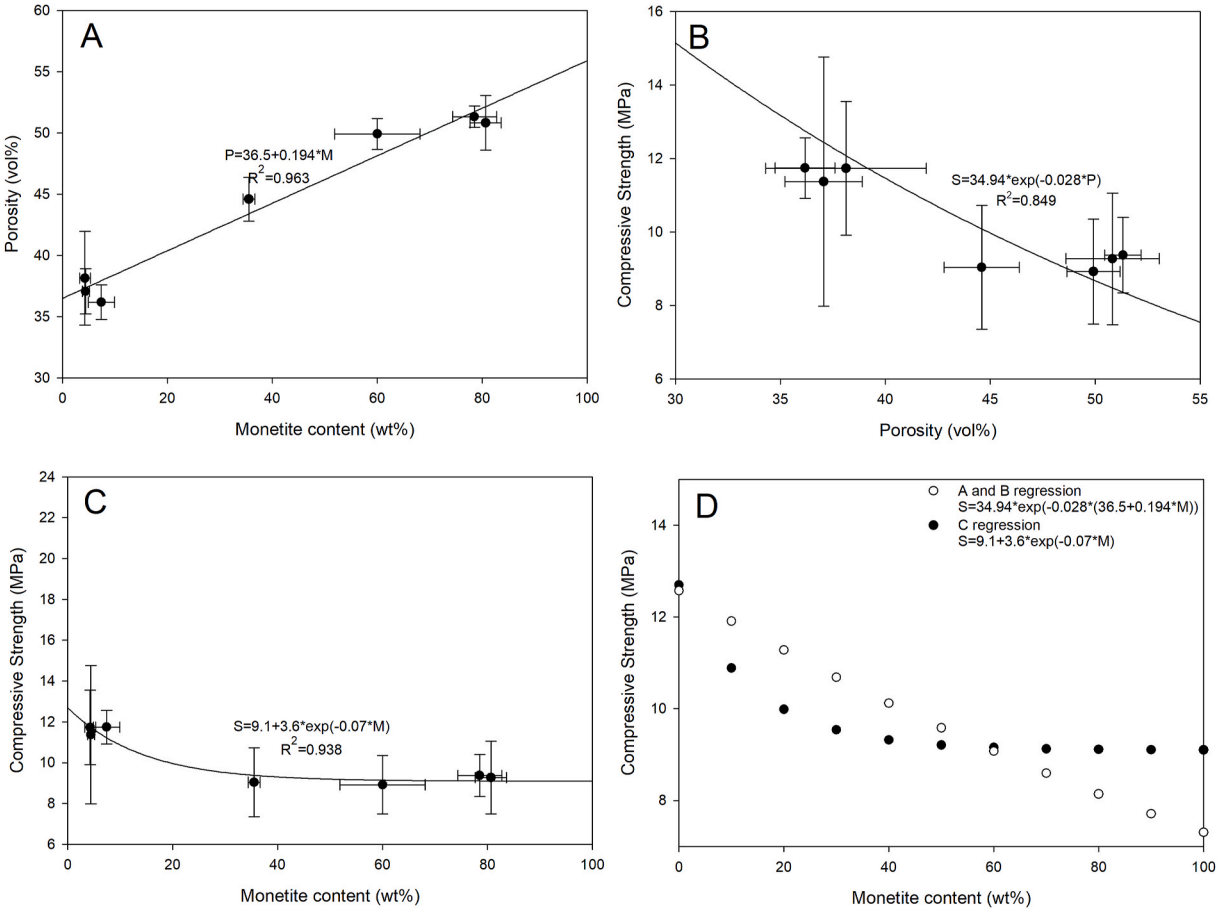

Fig. 4. The variations of (a) porosity in the microporous blocks with monetite content, (b) compressive strength with porosity, (c) compressive strength with monetite content; and (d) the comparison of the direct effect of monetite content on compressive strength with indirect effect derived from the dependency of porosity on monetite content and the direct effect of porosity on compressive strength.

depending on the pore size and shape (de Groot, 1984; Liu, 1997a). The relationship derived from our measurements gives a stress concentration factor of 0.028, lower than expected for calcium phosphates:

$$S = 34.94 * e^{-0.028P\%} \quad (7)$$

where S is the ultimate compressive strength, 34.94 MPa is the zero-porosity strength of the cement blocks and 0.028 is the stress concentration factor. The constants obtained from this direct correlation of strength with porosity (Fig. 4b) are not within the expected range and this inaccuracy stems from the assumption that strength is only a function of porosity. On the other hand, phase analysis results show that the samples are a mixture of variable brushite and monetite weight fractions and the microporosity formation accompanies monetite formation (i.e. strength of these samples is a function of both phase transformation and porosity, the effect of the former being more direct). Fig. 4c exhibits this correlation which can be regressed better by a three-parameter exponential function in comparison to the Rice model:

$$S = 9.1 + 3.6 * e^{-0.07P\%} \quad (8)$$

where 9.1 MPa is the average compressive strength of pure monetite blocks with 56% maximum microporosity, 3.6 MPa can be considered as a reduced theoretical cement strength due to the incoherency between coexisting brushite and monetite structures and 0.07 is the stress concentration factor within the expected limits for porous calcium phosphates. The direct correlation of strength with monetite is compared in Fig. 4d with the indirect correlation that is obtained through combination of equations (5) and (7). The difference between the direct and the indirect correlations reflects the mechanically stabilizing effect of monetite formation opposing the detrimental effect of microporosity on strength such that monetite formation improves strength above about 60% extent which is attributed to the higher coherency in the multiphase structure and the hypothesized higher intrinsic strength of monetite crystals compared to that of brushite. This threshold corresponds to an ionic strength of more than 4M NaCl and any less is seen to result in a detrimental effect of the phase transformation on strength.

3.2. Determination of the maximum packing ratio of size distributed NaCl mixtures

Maximum packing ratio of 38 samples were calculated accordingly and the results are given in the supplementary data. It is generally seen that increasing the size distribution of the samples has a positive effect on the maximum packing ratio as expected. As seen in Fig. 5, maximum packing ratio for all samples lie within the range between 0.566 and 0.689. Some samples were not packed as efficiently as randomly packed uniform sized spheres. This is attributed to the prismatic nature of the NaCl particles that increases the contact area and the consequent friction among them. A few size distributions were seen to produce well packed structures that resulted in about 0.1 increase in maximum packing ratio compared to the random packing of spheres, which may be sufficient to double the strength of a porous ceramic block (Liu et al., 2006).

Analysis of variance results show that the experimental model was significant ($F(21, 16) = 3.054$, $p = 0.05$) and the particle size group less than 38 μm (−38), the size group less than 212 μm (−212), and combined size groups less than 53 μm and 75 μm (−53 and −75) are significant model terms. The 38 μm and 212 μm particle size groups were necessary to obtain a well packed structure and the 53 μm, 75 μm particle groups were effective in decreasing the maximum packing ratio significantly when used in combination. All other particle size groups and the combination of these factors were seen to have insignificant effect on the maximum packing ratio.

Equal additions of both −53 and −75 reduced the packing ratio as seen in Fig. 6 as the second and third graphs on the diagonal path compared to those on the horizontal and vertical axes. The response surface graphs were obtained from experimental data by utilizing the analysis feature of the experimental design software. The first graph on the upper left demonstrates the synergistic effect of −38 and −212 only. The second graphs on the X and Y axes were obtained from quarter part additions of the intermediate size groups compared to equal unit weights of −38 and −212 and the third graphs were obtained from half part additions of intermediates. Although addition of either of the intermediate groups slightly improves packing, maximum packing ratio

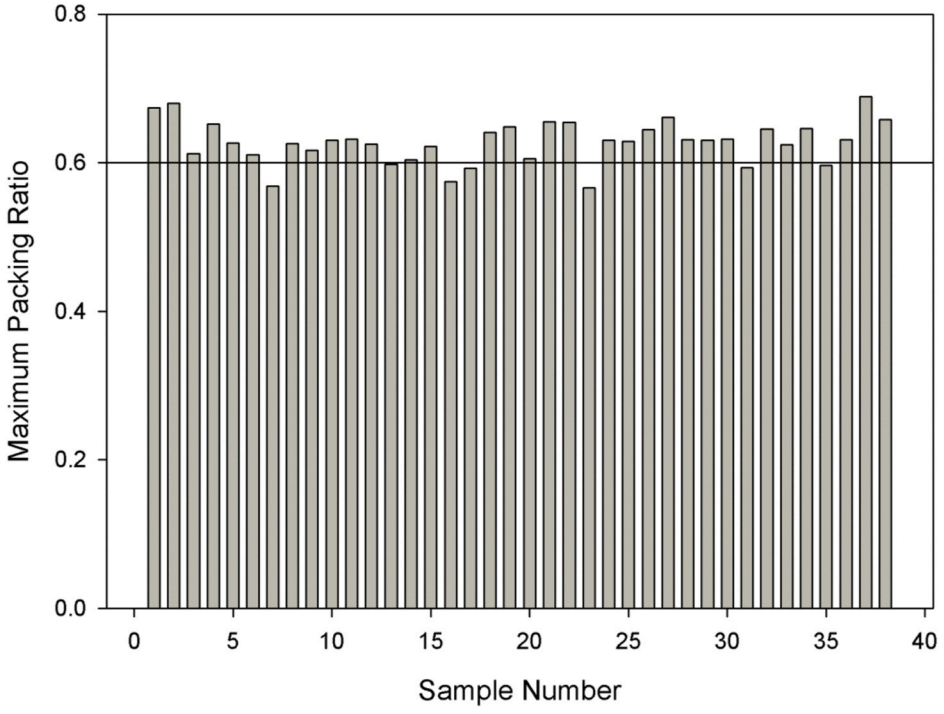

Fig. 5. Variation in maximum packing ratio of the samples. The reference line corresponds to the lower limit for the packing ratio of randomly packed uniform sized spheres.

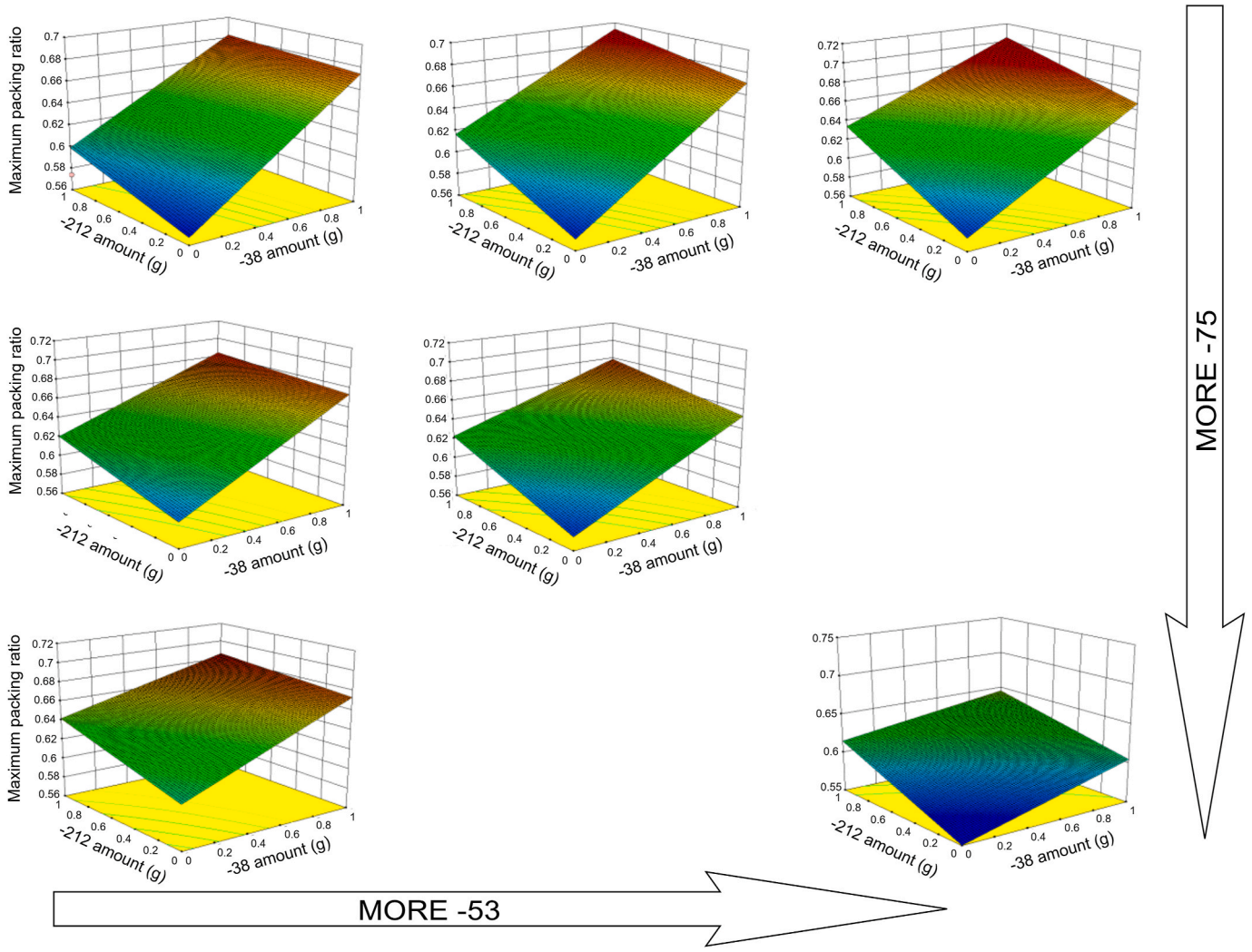

Fig. 6. Schematic representation of the synergistic and adverse effects of addition of −53, −75 μm NaCl particles in combination with the −38, −212 μm particles on packing ratio.

deteriorates significantly when all four particle size groups are added in equal amounts as seen at the bottom right of Fig. 6.

It is further observed that intermediate size groups are not effective in increasing the packing ratio when they are utilized as the largest particle group and a larger size group is necessary for effective packing. Rather the smaller intermediate size groups −53 and −75 generally improve packing when used in combination with −38 and −212. Such a beneficial effect is not seen for the particle size groups −106 and −150 because they interact with the largest particles instead of filling the gaps between them. Also they enable only moderate packing even in the presence of high number of fine particles under 38 μm.

The combination of the smallest and largest particle size groups constitutes a binary packing system that is well documented in the literature (Yu et al., 1997; Rassouly, 1999). Typically particle interaction effects are seen to diminish when the ratio between sizes of the larger and the finer particles exceed 7, which means that the local arrangement of an assembly of particles of one size is not disturbed by the vicinity of a particle of the second size (Kalyon and Aktaş, 2014). The maximum packing ratio for binary randomly packed spheres is reported to be 0.86 at an asymmetric coarse to fine particle size distribution of 73% coarse particles (de Larrard, 1999). The results of the rheometry study suggest a balanced size distribution of fine-intermediate-coarse particles of −38, −75, −212 as the optimum distribution (see supplementary data). As particle size groups in a ternary mixture differ in amount, interaction among different groups vary and an optimum interaction may be reached for maximum packing. This is parallel to the findings of Lam et al. where introduction of midsized particles effectly increased the packing ratio of a fine particle and coarse fiber binary mixture and the increase was more effective in the case of abundant coarse fibers with higher sizes (Lam, 1998). Similarly Yu et al. highlighted the importance of high midsized and coarse particle amount relative to finer particles on the packing ratio in the study on ternary mixture of alumina particles size distrubuted in the range of 3–100 μm (Yu et al., 1997). Positive effect of broadening the size distribution by adding another distinct size group, much finer than the −38 group on packing efficiency was observed upon further combining the size distributed NaCl porogens with fine calcium phosphate cement precursors in the subsequent part of this study.

3.3. Correlation between the microstructure and mechanical properties of microporous monetite-rich blocks

Archimedean, compositional and mechanical analyses of macroporous samples produced with the variable porogen size distribution approach generated a wealth of data that is presented in detail in the supplementary information. Furthermore, microstructure of these samples were revealed by examination of their fracture surfaces in SEM. For example the microstructure of a cement block from sample set 12 with a

balanced size distribution is presented in Fig. 7. Closely connected pores of a wide range of sizes from 30 to 200 μm are present in the cement matrix as seen in Fig. 7a and b. High magnification Fig. 7c shows the proximity of the pores that are separated by a few micrometers thick cement matrices. The highly porous structure and the dense struts provide effective toughening under compression similar to foamed ceramic matrix composites. Close-up image of the cement crystals in Fig. 7d reveals the monetite-rich microstructure with traces of sintered β-TCP particles which is in agreement with quantitative phase analysis results of about 80 wt% monetite and 15 wt% β-TCP.

The results of the Archimedean analysis of macroporous cement blocks show that broadening the solid size distribution by distinctly different size groups is effective in improving the packing ratio of porous cement blocks even further than the maximum packing ratio of the porogens. Increase in packing ratio with introduction of fine cement precursors was accompanied by reduction in total pore volumes, micropore volumes, sample volumes and microporosities compared to theoretically calculated values. Total pore and micropore volumes of macroporous blocks are given in Fig. 8a–b. Fig. 8c shows significant variations in packing improvements for all samples except set 37 as expected. It is worth noting that the porogens of this sample set had the highest maximum packing ratio and the addition of fine cement powder did not improve packing. Generally packing ratio of samples with porogen size distributions yielding low maximum packing ratio were significantly more enhanced compared to samples with porogen size distributions exhibiting already high maximum packing ratio in the rheometry analysis. Small improvement in packing densities of porous cement blocks consisting predominantly of finest porogen size groups indicate that fine porogen particles and finer cement precursors function similarly as void fillers between large porogen particles. This is expected as the finest porogen size group contains tailings that overlap with the size distribution of the finer cement powder.

The decrease in porosity of the cement blocks employing NaCl porogens can be attributed two sequential mechanisms: reduction of the packing defects by initial infiltration of cement precursors to the void spaces between coarser porogen particles, and densification of the cement matrix by local dissolution and precipitation of the cement precursors β-TCP, MCPM to nano-micrometer size monetite crystals in the space filled with cement setting liquid. It is assumed for the brushite forming cements that setting occurs before leaching of NaCl porogens due to their fast setting kinetics (Şahin and Kalyon, 2017). This assumption leads to the simplification of the macroporous cement processing into distict stages of mixing, setting and leaching, i.e. fine particles infiltrate before setting and packing defects within the cement matrix are densified by setting before leaching.

The mean estimated microporosity of the set cement blocks with no improvement in packing was around 37%, while the mean microporosity of the cement blocks with improved packing were found to be around 30%. The densification effect is expected to be even greater if the end product of the cement reaction was brushite rather than monetite (e.g. by the use of porogens that do not significantly increase the ionic strength of the setting liquid during setting). This is because complete monetite formation results in about 19% shrinkage of the cement structure due to its higher density than brushite and micropore formation around fine monetite crystals in a morphology resembling stacked-sheets. This additional micropore amount is found only in samples undergoing maximum conversion to monetite and the average of all the samples is lower due to the incomplete conversion of some samples.

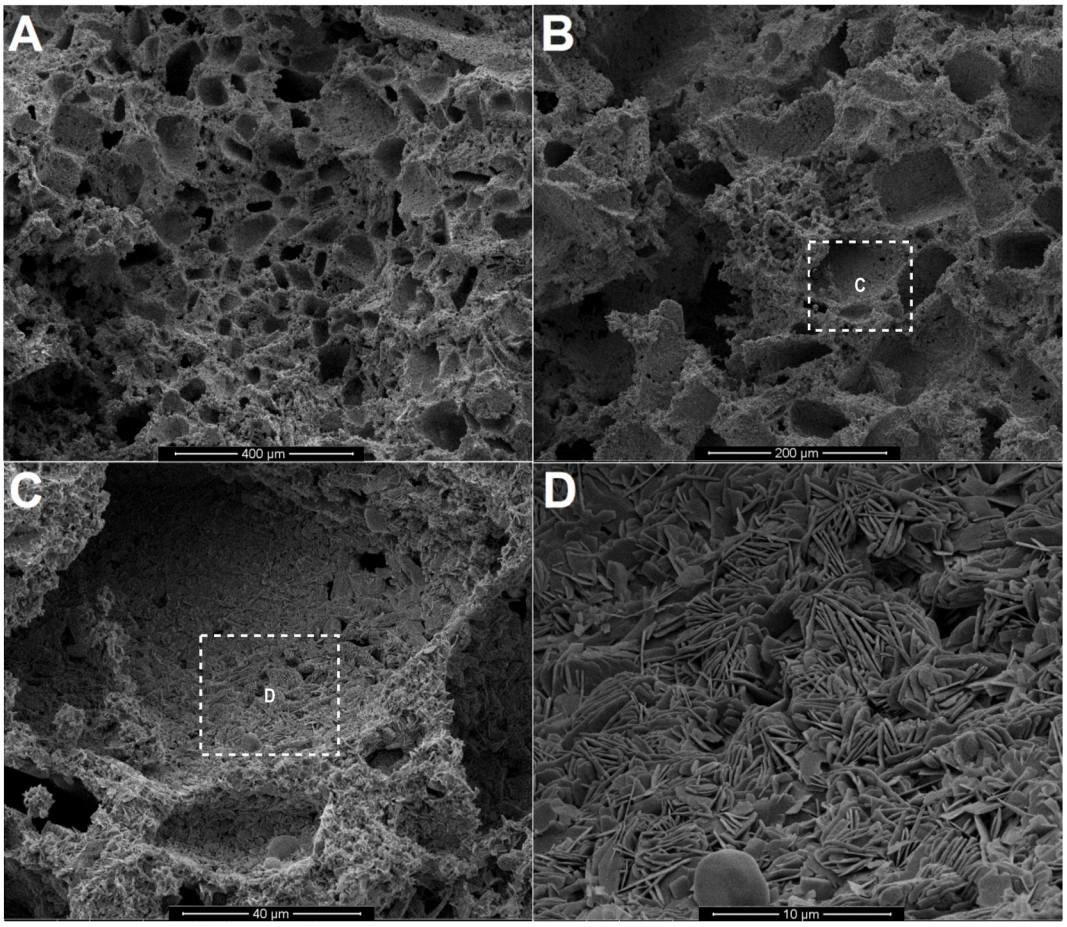

Fig. 7. SEM images of the fracture surface of macroporous cement sample number 12 with 250× magnification (A), 500× magnification (B), 2500× magnification (C), 10000× magnification (D).

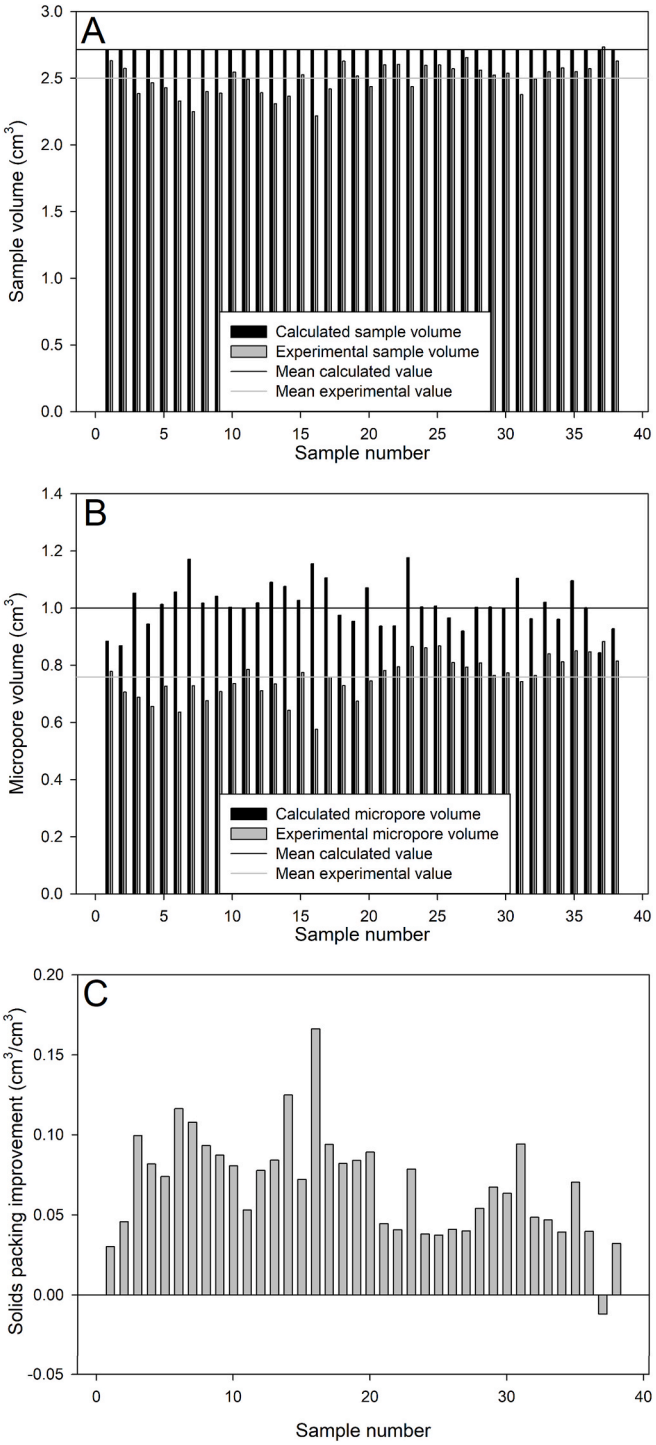

Fig. 8. Effect of size distribution of the solid phases on total pore volume (a) micropore volume (b) and solids packing improvement (c) of the porous cement block samples.

The phase analysis of the macroporous cement matrix given in Table 3 shows that monetite content of the samples ranges from 85 to 55% and relatively lower amounts of brushite and β-TCP are present. Data obtaied from monetite-rich macroporous cement block samples were isolated to observe the direct correlation between the porosities of monetite-rich macroporous cement blocks (containing higher than 80% monetite) and their solids packing densities (Fig. 9). A significant reduction in porosity of 10% was observed for the monetite-rich samples with the highest packing density (sample set 16) which suggests that

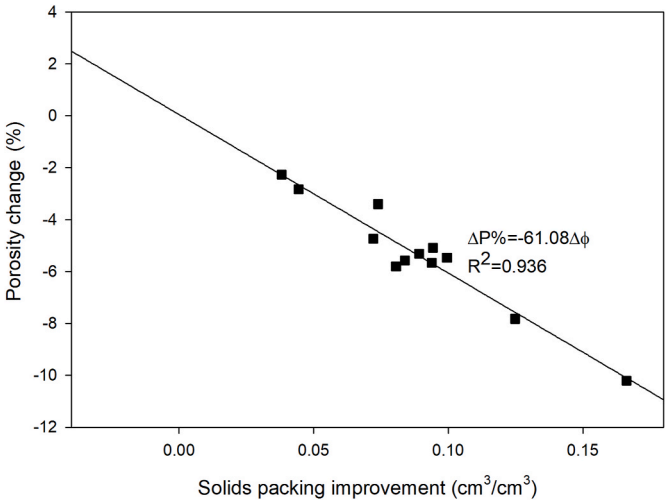

Fig. 9. Linear relationship between packing density and microporosity of samples containing higher than 80% monetite.

broadening the size distribution of cement precursors and porogens effectively counters the microporosity introduced to the structure during monetite formation. Thus, effective preparation of macroporous monetite cement blocks with dense matrices is possible, provided that the β-TCP residue, amounting in average to 11 wt% is reduced by additional means (e.g. by increasing the acidity and/or the amount of the setting liquid).

Slightly lower correlation between porosity, macroporosity and improvement in packing of all sample sets (see supplementary data for details) is due to variable monetite formation extents because of its direct proportionality with NaCl molarity of the setting liquid. There may form local gradients in saturation of the setting liquid with respect to NaCl due to phase migration and isolation effects which are expected to vary with size distribution and packing of NaCl porogens for different samples. The rate of dissolution and diffusion of NaCl molecules into the cement matrix depend on the concentration gradients in water kept at packing defects which is considered to be free from any convective effects during setting. On the other hand vigorous vibration for 1 min during the mixing stage ensured initial supersaturaion of the setting liquid with respect to NaCl. Therefore it can be hypothesized that setting liquid becomes undersaturated upon formation of monetite at high ionic strength due to exclusion of water from the crystals. Fast setting of monetite-rich cement is thought to result in isolation of the packing defects from the NaCl crystals, in effect to reduce their dissolution extent, the ionic strength of water and the extent of monetite formation as evident from the isolated macropores seen in the micrographs. On the other hand, there is the possibility of brushite to monetite conversion after setting, during the brief drying period. If dry conversion had any effect on the composition, it would be to improve the monetite conversion extent.

The sample and pore volume data obtained from Archimedean analysis in conjunction with quantitative phase analysis were converted to solids packing and porosity data with the assumption of negligible change in macropore volumes upon packing, setting and leaching. The validity of this approach is confirmed by the high correlation between packing and porosity despite the chemical effect of porogens. Pore volumes for all samples show the same dependence on micropore reduction by packing improvement due to broader size distribution regardless of the monetite content:

$$\Delta P = -3.65^{*}\Delta\varphi \quad (9)$$

Sample volumes were seen to vary more from the linear regression function of packing improvement which is attributed to defects generated on the surface of the cement blocks during the leaching process.

Some dissolution of calcium phosphate ions are expected to take place in water and weaken the integrity of surface cement matrix. Large porogen crystals were mostly trapped inside the blocks due to the surrounding liquid cement matrix during, so their volumes are assumed to mostly convert to macropores during cement processing.

The direct correlation between porosity and mechanical properties of the porous cement blocks were observed by isolating the compositional factor, monetite content and using a smaller sample group with monetite content higher than 80% as seen in Fig. 10. In this sample group microporous cement blocks with 45% porosity had a compressive strength around 9.5 MPa while the macroporous cement blocks with 66% porosity had a compressive strength around 2 MPa, close to the lower limtis of porosity and compressive strength of trabecular bone. Biomechanical analyses of trabecular bone in literature show highly scattered data according to the region of extraction and porosity, lower values of which have been found somewhere around 58% and 2 MPa respectively (Wang et al., 2015; Perilli et al., 2008; Brown et al., 2002), All mechanical properties measured under compressive loading obey Rice's model very well such that the exponential stress intensity factors are within the range of 3.5–10.8 ($*10^{-2}$) expected for porous calcium phosphates (Liu, 1997b). Theoretical compressive strength of dense monetite rich matrix is estimated around 330 MPa. For comparison, Hofmann et al. obtained a theoretical compressive strength around 85 MPa for uncompacted wet brushite cement blocks (Hofmann et al., 2009) and the regression of compressive strength data for size distributed brushite cement of Engstrand et al. gave a theoretical compressive strength around 165 MPa (Engstrand et al., 2014).

The relationship between mechanical properties and monetite content was not clear for the complete sample group due to the scattering in sample porosities and the consequent exponential variation in mechanical properties. Moreover, no correlation between the monetite content and the packing density was observed. Fluctuations in the monetite conversion extent do not seem to affect the dimensional and mechanical properties of the cement blocks significantly. Multiple mechanisms of microstructural evolution may be present including the initial packing, cement densification and conversion during drying that complicate the analysis of their effects. The most prominent mechanism of effective packing in the initial stages of cement setting is seen to indirectly affect the mechanical properties of porous cement blocks.

Analysis of subgroups of samples with the same porosity or monetite content did not give any correlation between packing density and mechanical properties. This is attributed to the experimental restriction of correlating porogen amount to the maximum packing ratio such that the effect of the reduction in micropore volume was negated by the rise in macropore volume with effective packing. On the other hand, this approach enabled calculation of theoretical strength of monetite-rich cements and proved the hypothesis that intrinsic strength of monetite crystals is higher than brushite.

4. Conclusion

Utilization of multifunctional ionic modifiers enabled controlled formation of monetite-rich micro- and macroporous cement blocks that are useful scaffold materials for orthopedic applications. Maximum packing ratio of various combinations of NaCl size distributions as determined by their rheological analysis were found to vary in a range between 57% and 69%. Statistical analysis revealed a positive correlation between the maximum packing ratio and the amount of −38 and −212 μm sized NaCl particle. The results of the Archimedean analysis reveal that combined solids size distribution is effective in improving the packing density of macroporous cement blocks even further than the maximum packing ratio ıf porogens. Increase in packing density with introduction of fine cement precursors was accompanied by reduction in sample volumes, total pore volumes and porosities. Despite the double dependence of porosity to packing density and monetite content, it was seen to decrease significantly with effective packing during monetite setting, roughly by 0.6% for every 1% increase in solids packing due to the broader size distribution of cement precursors and the NaCl particles. According to the fracture mechanics theory, the highest achieved porosity reduction of 10% is able to double the strength of the cement blocks. Compressive loading results confirmed this general exponential dependence of mechanical properties to porosity with greater correlation for monetite-rich samples without phase variations. Theoretical

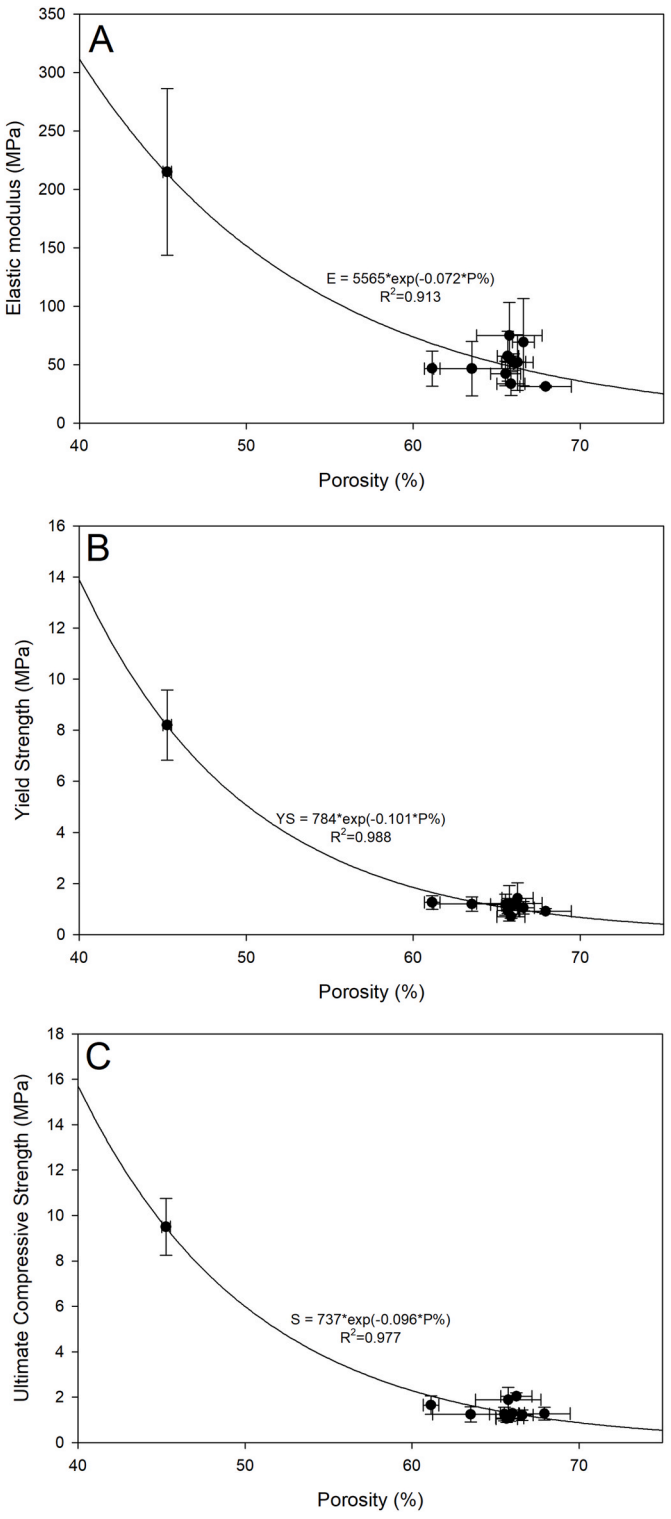

Fig. 10. Correlation between porosity and mechanical properties of samples containing monetite content higher than 80% tested under comporession: a) elastic modulus, b) yield strength, c) ultimate strength.

compressive strength of fully dense monetite-rich matrix is calculated as around 330 MPa, greater than the theoretical strength of brushite cements reported previously. Thus, introduction of a broad size distribution to monetite forming cement precursors and NaCl porogens effectively counteracts the microporosity introduced to the structure during monetite formation and is supposed to be an appropriate strategy towards developing robust monetite cement scaffolds for orthopedic applications.

CRediT authorship contribution statement

Erdem Şahin: Conceptualization, Methodology, Software, Validation, Formal analysis, Investigation, Data curation, Writing - original draft, Writing - review & editing, Visualization. **Muhsin Çiftçioğlu:** Resources, Writing - review & editing, Supervision, Project administration.

Declaration of competing interest

The authors declare that they have no known competing financial interests or personal relationships that could have appeared to influence the work reported in this paper.

Acknowledgements

We would like to thank Deniz Ekerler and Sun Chemical Inc. For their contribution in particle size measurements and the staff of Materials Research Center at IZTECH for their assistance in characterization runs.

Appendix A. Supplementary data

Supplementary data to this article can be found online at https://doi.org/10.1016/j.jmbbm.2021.104363.

References

Aiqin, W., Chengzhi, Z., Ningsheng, Z., 1997. Cement Concr. Res. 27, 685–695.
Ajaxon, I., Acciaioli, A., Lionello, G., Ginebra, M.P., Öhman-Mägi, C., Baleani, M., Persson, C., 2017. Elastic properties and strain-to-crack-initiation of calcium phosphate bone cements: revelations of a high-resolution measurement technique. Journal of the mechanical behavior of biomedical materials 74, 428–437.
Ajaxon, Ingrid, Caroline Öhman Mägi, CeciliaPersson, 2017. Compressive fatigue properties of an acidic calcium phosphate cement—effect of phase composition. J. Mater. Sci.: Mater. Med. 28 (3), 41.
Alshaaer, M., Cuypers, H., Rahier, H., Wastiels, J., 2011. Production of monetite-based Inorganic Phosphate Cement (M-IPC) using hydrothermal post curing (HTPC). Cement Concr. Res. 41 (1), 30–37.
Bentz, D.P., Garboczi, E.J., Haecker, C.J., Jensen, O.M., 1999. Cement Concr. Res. 29, 1663–1671.
Bohner, M., Gbureck, U., 2008. J. Biomed. Mater. Res. B Appl. Biomater. 84B, 375–385.
Bohner, M., Merkle, H.P., Lemaitre, J., 2000. J. Mater. Sci. Mater. Med. 11, 155–162.
Brown, S.J., Pollintine, P., Powell, D.E., Davie, M.W., Sharp, C.A., 2002. Regional differences in mechanical and material properties of femoral head cancellous bone in health and osteoarthritis. Calcif. Tissue Int. 71 (3), 227–234.
Cama, G., Gharibi, B., Sait, M.S., Knowles, J.C., Lagazzo, A., Romeed, S., Di Silvio, L., Deb, S., 2013. J. Mater. Chem. B 1, 958–969.
Canal, C., Ginebra, M.P., 2011. Fibre-reinforced calcium phosphate cements: a review. Journal of the mechanical behavior of biomedical materials 4 (8), 1658–1671.
de Groot, K., 1984. Chapter 23, calcium phosphate ceramics: their current status. In: Contemporary Biomaterials. William Andrew Publishing/Noyes.
de Larrard, F., 1999. Concrete Mixture Proportioning: a Scientific Approach. Taylor&Francis.
Desai, Tarang R., Bhaduri, Sarit B., Cuneyt Tas, A., 2007. A self-setting, monetite (CaHPO 4) cement for skeletal repair. In: Ceramic Engineering and Science Proceedings, vol. 27. American Ceramic Society. No. 6.
Dorozhkin, S.V., 2008. J. Mater. Sci. 43, 3028–3057.
Engstrand, Johanna, Persson, Cecilia, Engqvist, Håkan, 2014. The effect of composition on mechanical properties of brushite cements. Journal of the mechanical behavior of biomedical materials 29, 81–90.
Espanol, M., Perez, R.A., Montufar, E.B., Marichal, C., Sacco, A., Ginebra, M.P., 2009. Acta Biomater. 5, 2752–2762.
Frigione, G., Marra, S., 1976. Cement Concr. Res. 6, 113–127.
Galea, L.G., Bohner, M., Lemaître, J., Kohler, T., Müller, R., 2008. Bone substitute: transforming β-tricalcium phosphate porous scaffolds into monetite. Biomaterials 29 (24–25), 3400–3407.
Gbureck, U., Dembski, S., Thull, R., Barralet, J.E., 2005. Biomaterials 26, 3691–3697.
Gbureck, U., Hölzel, T., Klammert, U., Wuerzler, K., Mueller, F.A., Barralet, J.E., 2007. Resorbable dicalcium phosphate bone substitutes prepared by 3D powder printing. Adv. Funct. Mater. 17 (18), 3940–3945.
Geffers, M., Barralet, J.E., Groll, J., Gbureck, U., 2015. Dual-setting brushite–silica gel cements. Acta Biomater. 11, 467–476.
Hofmann, M.P., Mohammed, A.R., Perrie, Y., Gbureck, U., Barralet, J.E., 2009. Acta Biomater. 5, 43–49.
http://www.mindat.org/min-2755.html.
https://www.mindat.org/min-793.html.
Jones, A.C., Arns, C.H., Hutmacher, D.W., Milthorpe, B.K., Sheppard, A.P., Knackstedt, M.A., 2009. Biomaterials 30, 1440–1451.
Kalyon, D.M., Aktaş, S., 2014. Factors affecting the rheology and processability of highly filled suspensions. Annual review of chemical and biomolecular engineering 5, 229–254.
Kendall, K., Howard, A.J., Birchall, J.D., 1983. The relation between porosity, microstructure and strength, and the approach to advanced cement-based materials. Phil. Trans. Roy. Soc. Lond. Math. Phys. Sci. 310 (1511), 139–153.
Klammert, U., Reuther, T., Jahn, C., Kraski, B., Kübler, A.C., Gbureck, U., 2009. Cytocompatibility of brushite and monetite cell culture scaffolds made by three-dimensional powder printing. Acta Biomater. 5 (2), 727–734.
Kwan, A.K.H., Fung, W.W.S., 2009. Cement Concr. Compos. 31, 349–357.
Lam, D.C.C., 1998. J. Mater. Process. Technol. 79, 170–176.
Liu, D.M., 1997a. Influence of porosity and pore size on the compressive strength of porous hydroxyapatite ceramic. Ceram. Int. 23, 135–139.
Liu, D.M., 1997b. Ceram. Int. 23, 135–139.
Liu, D.M., 1998. Preparation and characterisation of porous hydroxyapatite bioceramic via a slip-casting route. Ceramics Inkmational24 441–446.
Liu, D.M., 2000. J. Mater. Sci. 35, 5503–5507.
Liu, C., Shao, H., Chen, F., Zheng, H., 2006. Biomaterials 27, 5003–5013.
Öhman, C., Unosson, J., Carlsson, E., et al., 2015. Porosity prediction of calcium phosphate cements based on chemical composition. J. Mater. Sci. Mater. Med. 26, 210. https://doi.org/10.1007/s10856-015-5497-0.
Perilli, E., Baleani, M., Öhman, C., Fognani, R., Baruffaldi, F., Viceconti, M., 2008. J. Biomech. 41, 438–446.
Rassouly, S.M.K., 1999. Powder Technol. 103, 145–150.
Rice, R.W., 1998. Porosity of Ceramics. Marcel Dekker, Inc, p. 276.
Rossi, R.C., 1968. Prediction of elastic moduli of composites. J. Am. Ceram. Soc. 51 8, 433–439.
Şahin, Erdem, 2018. Calcium phosphate bone cements. Cement Based Materials 191.
Sahin, E., Ciftcioglu, M., 2013. J. Mater. Chem. B 1, 2943–2950.
Şahin, E., Çiftçioğlu, M., 2014. Mater. Res. Innovat. 18 (3), 138–145.
Şahin, Erdem, Kalyon, Dilhan M., 2017. The rheological behavior of a fast-setting calcium phosphate bone cement and its dependence on deformation conditions. Journal of the mechanical behavior of biomedical materials 72, 252–260.
Sivakumar, G.R., Girija, E.K., Kalkura, S.N., Subramanian, C., 1998. Cryst. Res. Technol. 33, 197–205.
Takagi, S., Chow, L.C., 2001. J. Mater. Sci. Mater. Med. 12, 135–139.
Tamimi, F., Torres, J., Kathan, C., Baca, R., Clemente, C., Blanco, L., Lopez Cabarcos, E., 2008. J. Biomed. Mater. Res. 87, 980–985.
Tamimi, F., Torres, J., Bassett, D., Barralet, J., Cabarcos, E.L., 2010. Resorption of monetite granules in alveolar bone defects in human patients. Biomaterials 31 (10), 2762–2769.
Tamimi, F., Le Nihouannen, D., Eimar, H., Sheikh, Z., Komarova, S., Barralet, J., 2012a. The effect of autoclaving on the physical and biological properties of dicalcium phosphate dihydrate bioceramics: brushite vs. monetite. Acta Biomater. 8 (8), 3161–3169.
Tamimi, F., Sheikh, Z., Barralet, J., 2012b. Dicalcium phosphate cements: brushite and monetite. Acta Biomater. 8 (2), 474–487.
von Doernberg, M.C., von Rechenberg, B., Bohner, M., Grunenfelder, S., van Lenthe, G. H., Muller, R., Gasser, B., Mathys, R., Baroud, G., Auer, J., 2006. Biomaterials 27, 5186–5198.
Wang, Nancollas, G.H., 2008. Calcium orthophosphates: crystallization and dissolution. Chem. Rev. 108, 4628–4669.
Wang, J., Zhou, B., Liu, X.S., Fields, A.J., Sanyal, A., Shi, X., et al., 2015. Trabecular plates and rods determine elastic modulus and yield strength of human trabecular bone. Bone 72, 71–80.
Xu, H.H., Quinn, J.B., 2002. Biomaterials 23, 193–202.
Xu, H.H., Quinn, J.B., Takagi, S., Chow, L.C., Eichmiller, F.C., 2001. J. Biomed. Mater. Res. 57, 457–466.
Yu, A.B., Bridgwater, J., Burbidge, A., 1997. Powder Technol. 92, 185–194.